AIAA 79-1565R

Transonic Flow Calculations over Two-Dimensional Canard-Wing Systems

Vijaya Shankar* and Norman D. Malmuth†
Rockwell International Science Center, Thousand Oaks, Calif.
and
Julian D. Cole‡
University of California, Los Angeles, Calif.

As a prototype for the three-dimensional interaction problem, the transonic interference flowfields over two-dimensional canard-wing systems are computed using transonic small disturbance theory. In the calculation, the two airfoils comprising the lifting "biplane" system are placed in separate computational planes with an overlapped region across which information from one airfoil to the other is transferred at the end of each relaxation cycle. Results showing the favorable interference in overall lift are presented and compared with linear theory calculations. Far field expressions for solid, slotted, and free jet wind tunnel wall cases that correspond to the canard-wing arrangement are also described.

Nomenclature

A,B	= constants appearing in Eq. (13)
C	= chord, constant appearing in Eq. (13)
C_p	= pressure coefficient
C_L	= lift coefficient
D	= vertical gap between lifting elements
$f(x)$	= function describing shape of lifting surface
G	= Green's function
H	= tunnel half height
H_C, H_W	= distances defined in Fig. 3
I_D, I_T, I_W, I_{wa}	= integrals defined in Eq. (6)
K	= transonic similarity parameter
M_∞	= freestream Mach number
S	= stagger
$t(x)$	$= f_u - f_\ell$
u	$= \phi_x$
$x, \bar{y}$	= transonically scaled Cartesian coordinates
$y_n(y)$	= eigenfunction appearing in Green's function
Y	$= \sqrt{K}\bar{y}$
α	= angle of attack
Γ	= circulation
δ	= flow deflection parameter
$\delta(x)$	= delta function
η	= dummy variable for Y
θ	$= \tan^{-1}(Y/x)$
λ_n	= eigenvalues appearing in Green's functions
λ	= root of secular equation for eigenvalues λ_n
μ	= scaled porosity parameter
ξ	= dummy variable for x
ϕ	= perturbation velocity potential

Subscripts and Superscripts

C	= canard
D	= doublet
W	= wing
wa	= wake
CU	= canard upper surface
CL	= canard lower surface
WU	= wing upper surface
WL	= wing lower surface

Presented as Paper 79-1565 at the AIAA 12th Fluid and Plasma Dynamics Conference, Williamsburg, Va., July 23-25, 1979; submitted Nov. 2, 1979; revision received April 1, 1980.

*Member Technical Staff, Mathematical Science Group. Member AIAA.
†Project Manager, Fluid Dynamics. Associate Fellow AIAA.
‡Professor. Fellow AIAA.

I. Introduction

A NUMBER of highly maneuverable fighter configurations such as HiMAT, AFTI, and XFV-12A have been proposed with closely coupled canard systems which can lead to advantages in trim drag reduction at transonic speeds. Additional advantages associated with improved side force capability have been described by Re and Capone.[1] The associated interaction due to such surfaces with the wing as well as those from conventional tail planes involves important nonlinear phenomena in the supercritical speed regime. These effects can significantly change spanwise load distributions as well as the effective incidence field. Corresponding modifications of aerodynamic performance and stability characteristics are therefore to be anticipated not only for fighter configurations, but large-aspect-ratio systems typical of transport arrangements as well.

To understand clearly the closely coupled canard-wing interference flowfields with emphasis on benefits associated with longitudinal positioning that have been discussed in the subsonic regime by Lacey,[2] initially, a two-dimensional model is studied in the nonlinear context of the present investigation. Here a computational solution of the Kármán-Guderley transonic small disturbance model[3] with perturbation velocity potential as the dependent variable is utilized to provide pressure distributions on the airfoil surfaces. The drag estimate using the small disturbance theory is somewhat questionable due to the breakdown of the theory near the nose of the airfoil, especially for thick configurations. Accordingly, lift estimates are emphasized in this paper.

Results are presented for several canard-wing configurations and for different Mach numbers and angles of attack. For certain canard-wing arrangements there is clear indication of lift augmentation which is helpful in achieving increased trimmed-lift capability. To exhibit shock interference phenomena associated with this bi-wing system, results are compared with linear theory calculations.

The extension of the present work to three-dimensional closely coupled canard-wing systems is currently in progress, and uses many of the concepts applied in this paper.

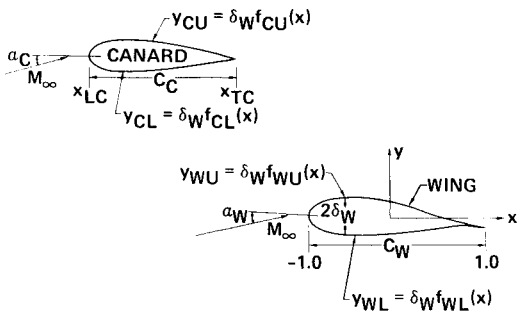

Fig. 1 Two-dimensional canard-wing arrangement.

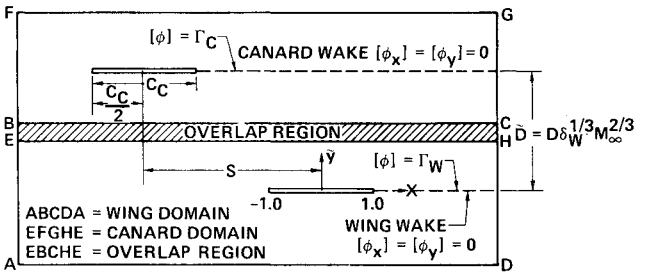

Fig. 2 Computational setup showing separate domains for the canard and the wing.

II. Formulation

Figure 1 shows a typical two-dimensional canard-wing arrangement. The parameters α_C, C_C and α_W, C_W represent the angle of attack and the chord length of the canard and the wing airfoil, respectively. The thickness parameter δ_W of the wing airfoil is used in defining both the canard and the wing airfoil ordinates as

$$y_{CU,CL} = \delta_W f_{CU,CL}(x) - \alpha_C x \quad \text{defines the canard}$$

$$y_{WU,WL} = \delta_W f_{WU,WL}(x) - \alpha_W x \quad \text{defines the wing} \qquad (1)$$

The small disturbance Kármán-Guderley equation[3]

$$[K-(\gamma+1)\phi_x]\phi_{xx} + \phi_{\tilde{y}\tilde{y}} = 0 \qquad (2)$$

is used to study this problem. The quantity $K=(1-M_\infty^2)/M_\infty \delta_W^{2/3} \tilde{y} = y\delta_W^{1/3} M_\infty^{2/3}$ is the scaled vertical coordinate. The associated boundary condition on the canard-wing airfoils becomes

$$(\phi_{\tilde{y}})_{CU,CL} = \frac{df_{CU,CL}(x)}{dx} - \frac{\alpha_C}{\delta_W}$$

$$(\phi_{\tilde{y}})_{WU,WL} = \frac{df_{WU,WL}(x)}{dx} - \frac{\alpha_W}{\delta_W} \qquad (3)$$

Figure 2 shows the idealized domains of the problem. The two airfoils are separated by a distance D in the vertical direction. In terms of the scaled vertical coordinate, this becomes $\tilde{D} = D\delta_W^{1/3} M_\infty^{2/3}$. The distance between the center points of the canard and the wing chord in the x direction is S. As a model for the three-dimensional problem where different shearing transformations are to be used for the canard and the wing depending on their planform geometry, in the two-dimensional formulation, the physical domain is split into two separate subregions, one containing the wing (ABCDA) and the other containing the canard (EFGHE). The subdomains have a common overlapped region (EBCHE) across which transfer of nonlinear information from one domain to the other will take place. To complete the formulation, an

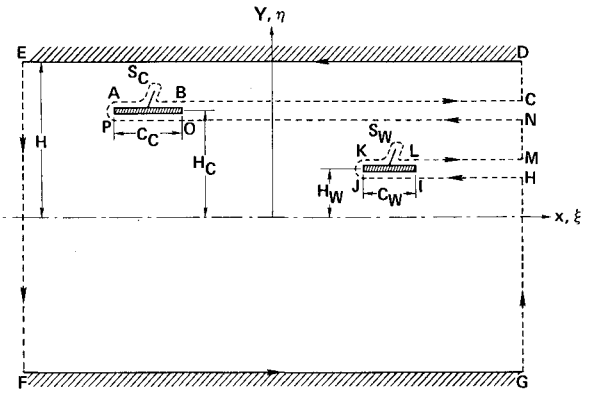

Fig. 3 Cut region for application of Green's theorem.

asymptotic far field in terms of the perturbation potential ϕ is prescribed along the outer boundary AFGDA. Retaining only the dominant terms, the far field expression is given by

$$\phi_{FF} = -\frac{\Gamma_C \theta_C}{2\pi} - \frac{\Gamma_W \theta_W}{2\pi} + \ldots \qquad (4)$$

where

$$\theta_C = \tan^{-1}[\sqrt{K}(\tilde{y}-\tilde{D})/(x-S)] \qquad \theta_W = \tan^{-1}(\sqrt{K}\tilde{y}/x)$$

with $(x,\tilde{y})$ being any point in the far field, and Γ_C and Γ_W are the circulations around the canard and the wing, respectively. Because of nonlinear interference, Γ_C and Γ_W will take on different values than those associated with isolated airfoils.

Equation (2) along with the boundary condition Eq. (3) and the far field condition Eq. (4) is solved separately in the wing and the canard domain using the Murman and Cole[3] operator modified to include Jameson's pseudotime operator.[4] At the end of each relaxation cycle, the values of velocity potential ϕ along the top boundary of the wing domain (BC in Fig. 2) are obtained by interpolating the ϕ field in the canard domain. This interpolated value serves as the Dirichlet boundary condition for the next iteration. Similarly, the values of ϕ along the bottom boundary of the canard domain (E-H in Fig. 2) are obtained from the wing domain. In this manner, the overlap region transfers the nonlinear interaction between the canard and the wing airfoil. When the shock from the canard and/or the wing crosses the overlap region, at grid points on BC and EH neighboring the shock, proper one-sided extrapolation for ϕ is implemented to allow for the jump in ϕ_x across the shock. Once the relaxation process converges, the pressure coefficient C_p and the lift coefficient C_L on the canard and the wing are calculated from

$$C_p = -2(\delta_W^{1/3}/M_\infty^{3/4})\phi_x \qquad (C_L)_{W,C} = (\delta_W^{1/3}/M_\infty^{3/4})\Gamma_{W,C} \qquad (5)$$

Tunnel Far Fields

The far field expression given by Eq. (4) is applicable only to the free flight case. For solid, slotted, or free jet wind tunnel wall cases, the downstream and upstream far field conditions have to be properly modeled. An outline of the derivation will be provided in what follows for these cases. The detailed analysis and treatment of porous walls will be given elsewhere. The procedure to be discussed contrasts with that employed in Refs. 5 and 6, which assumes by analogy to the free field case that the wind-tunnel asymptotic has a dominant structure consisting of a doublet and vortex in the asymptotic Prandtl-Glauert flow subject to the wall conditions. In this connection, the solution for a subsonic compressible vortex between porous walls is given in Ref. 7. Although the doublet-vortex assumption is plausible, it is not made in the approach herein. Rather, this structure is confirmed as the dominant term of an asymptotic expansion

based on a systematic approximate solution of the nonlinear integrodifferential equation of the confined flow. In the complete analysis to be presented in another paper, it will also be shown that the heuristic approach of Ref. 5 cannot give important nonlinear couplings and feedbacks that appear as second-order terms obtained from the systematic expansion procedure based on the integrodifferential equation.

The appropriate asymptotic expressions can be obtained by utilization of Green's theorem on the region in Fig. 3 or on an integration by parts procedure, as applied in Ref. 8 for a single airfoil symmetrically situated in a solid tunnel and application of a suitable Green's function G designed to remove certain wall boundary terms in the resulting integral equation which can be written as

$$\phi_{FF}=I_D+I_T^{(W)}+I_T^{(C)}+I_W^{(W)}+I_W^{(C)}+I_{wa}^{(W)}+I_{wa}^{(C)}+I_E \qquad (6)$$

where

$$I_D=\frac{-(\gamma+1)}{2K}\int_{-H}^{H}d\eta\int_{-\infty}^{\infty}u^2\frac{\partial G}{\partial\xi}\,d\xi \quad =\text{nonlinear doublet}$$

$$I_T^{(W)}=\int_{x_K}^{x_L}t_W'(\xi)G(\xi,H_W;x,Y)\,d\xi \quad =\text{thickness effect of wing}$$

$$I_T^{(C)}=\int_{x_A}^{x_B}t_C'(\xi)G(\xi,H_C;x,Y)\,d\xi \quad =\text{thickness effect of canard}$$

$$I_W^{(W)}=-\int_{x_K}^{x_L}[\phi]_W\left(\frac{\partial G}{\partial\eta}\right)\Big|_{\eta=H_W}d\xi \quad =\text{doublet effect of wing}$$

$$I_W^{(C)}=-\int_{x_A}^{x_B}[\phi]_C\left(\frac{\partial G}{\partial\eta}\right)\Big|_{\eta=H_C}d\xi \quad =\text{doublet effect of canard}$$

$$I_{wa}^{(W)}=-\Gamma_W\int_{x_L}^{\infty}\left(\frac{\partial G}{\partial\eta}\right)\Big|_{\eta=H_W}d\xi \quad =\text{wake doublet of wing}$$

$$I_{wa}^{(C)}=-\Gamma_C\int_{x_B}^{\infty}\left(\frac{\partial G}{\partial\eta}\right)\Big|_{\eta=H_C}d\xi \quad =\text{wake doublet of canard}$$

$$I_E=\int_{-H}^{H}\left(\phi\frac{\partial G}{\partial\xi}\right)_{\xi=\infty}d\xi$$

Here, W and C superscripts and subscripts refer to the wing and canard, respectively, and Γ = circulation; $H=\tilde{H}\sqrt{K}$ where $\tilde{H}$ is the scaled tunnel half height, $Y=\sqrt{K}\tilde{y}$; $u=\phi_x$; $t_C=f_{CU}-f_{CL}$; $t_W=f_{WU}-f_{WL}$; $[\ ]_w=(\ )H_W^+-(\ )H_W^-$; $[\ ]_C=(\ )H_C^+-(\ )H_C^-$; and G is a Green's function to be defined presently.

The wall conditions based on Baldwin[9] are

$$\phi\pm\mu\phi_Y=0 \qquad \text{on} \quad Y=\pm H \qquad (7)$$

$\mu\to 0$ free jet $\qquad \mu\to\infty$ solid wall

Here μ is a scaled slot parameter. Actually, Eq. (7) is an integrated form (with respect to x) of the relations utilized in Ref. 9 and applied in Refs. 10 and 11, with the assumption that $\phi(-\infty,Y)=0$. From the nonuniqueness of the integral representation arising in Eq. (6), in particular the term I_E, some additional assumption of this type about the entrance flow inclination is required to achieve uniqueness.

One key problem in obtaining an asymptotic solution of Eq. (6) for $x\to\infty$ is the determination of the Green's function G. In accord with previous remarks, the most advantageous Green's function to be used in Eq. (6) is selected to satisfy Eq. (7) and

$$G_{xx}+G_{YY}=\delta(x-\xi)\delta(Y-\eta)$$

Thus, G corresponds to the potential of a point source subjected to given wall conditions, and is given by

Solid wall

$$G=\frac{|x-\xi|}{4H}-\frac{1}{2H}\sum_{n=1}^{\infty}\frac{e^{-\lambda_n|x-\xi|}}{\lambda_n}\cos\lambda_n(Y+H)\cos\lambda_n(\eta+H)$$

$$\lambda_n=(n\pi/2H) \qquad (8)$$

Slotted wall and free jet

$$G=-\tfrac{1}{2}\sum_{n=1}^{\infty}\frac{e^{-\lambda_n|x-\xi|}y_n(Y)y_n(\eta)}{\lambda_n[(\lambda_n^2+\mu^{-2})H+\mu^{-1}]}$$

$$y_n(y)=(\lambda_n\cos\lambda_nH+\mu^{-1}\sin\lambda_nH)\cos\lambda_nY$$

$$+(\lambda_n\sin\lambda_nH-\mu^{-1}\cos\lambda_nH)\sin\lambda_nY \qquad (9)$$

and the λ_n's are the roots λ of the following transcendental equation

$$\tan 2\lambda H=(2\lambda\mu/\lambda^2\mu^2-1)$$

where

$$\lambda_1<\lambda_2<\lambda_3\cdots\lambda_n<\cdots\infty$$

It should be noted that the free jet case ($\mu\to 0$) is contained in Eq. (9) but the solid wall ($\mu\to\infty$) corresponding to Eq. (8) is not.

On substitution of Eqs. (8) and (9) into Eq. (6) using $\phi(-\infty,Y)=0$ to evaluate I_E, we obtain the following results for ϕ_{FF} by approximating the various integrals for $x\to\infty$ which are correct to within exponentially small terms with arguments proportional to $\lambda_n x$:

Solid tunnel

$$\phi_Y(x,\pm H)=0$$

$$\phi_{FF}=\Gamma_C+\frac{\Gamma_W}{2}+\phi_D+\ldots, \qquad H_C<Y\le H$$

$$=\frac{\Gamma_W}{2}+\phi_D+\ldots, \qquad H_W<Y<H_C$$

$$=-\frac{\Gamma_W}{2}+\phi_D+\ldots, \qquad -H\le Y\le H_W \qquad (10)$$

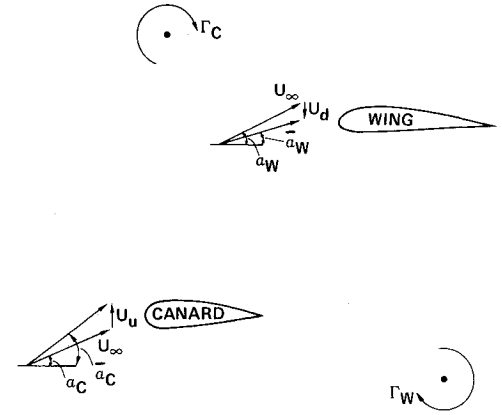

Fig. 4 Schematic of a) effect of canard on the wing; b) effect of wing on the canard.

where ϕ_D is the doublet contribution given by

$$4KH\phi_D = \int_{x_A}^{x_B} t_C(\xi)\,d\xi + \int_{x_K}^{x_L} t_W(\xi)\,d\xi + \frac{\gamma+1}{2K}\int_{-H}^{H} d\eta \int_{-\infty}^{\infty} u^2(\xi,\eta)\,d\xi \tag{11}$$

Slotted and free jet tunnel [Eq. (7)]

$$\phi_{FF} = \frac{(\Gamma_W+\Gamma_C)}{2}\left\{1-\frac{Y}{\mu+H}\right\}+\ldots, \qquad H_C < Y \le H$$

$$= \tfrac{1}{2}\left\{\Gamma_W-\Gamma_C-\frac{(\Gamma_W+\Gamma_C)\,Y}{\mu+H}\right\}+\ldots, \qquad H_W < Y < H_C$$

$$= -\frac{(\Gamma_W+\Gamma_C)}{2}\left\{1-\frac{Y}{\mu+H}\right\}+\ldots, \qquad -H \le Y \le H_W \tag{12}$$

In Eqs. (10) and (12), the terms involving Γ_C and Γ_W arise directly from the wake doublet integrals $I_{wa}^{(W,C)}$ appearing in Eq. (6). These are $\mathcal{O}(1)$ as $x\to\infty$ for all wall conditions. The doublet term ϕ_D arises from $I_D, I_Y^{(W,C)}$. This term is exponentially small for the slotted wall and free-jet cases as are the other integrals.

The higher order terms in the sequence approximating the solution of Eq. (6) involve terms of the type

$$e^{-\lambda_n x}\int_0^x e^{\lambda_n \xi} u^2\,d\xi$$

These integrals can be approximated for $x\to\infty$ by an asymptotic expansion based on the convolution theorem for Laplace transforms. We note also that the results Eqs. (10) and (12) could be obtained by assuming the following linear polynomial solution of the asymptotically (scaled) harmonic field:

$$\phi = Ax + BY + C \quad \text{as} \quad x\to\infty, \quad (A,B \text{ constants}) \tag{13}$$

where C is a discontinuous constant adjusted to satisfy the potential jumps across the canard and wing wakes. This procedure leads to certain nonuniquenesses. The nonlinear analysis appears to be the only means of resolving these ambiguities by providing the necessary coupling with the near field.

We also note that the present analysis can be extended to treat multiple lifting units using a similar procedure. A typical example is a cascade of turbine blades in a duct.

For the porous case, the eigenvalues λ_n appear in the boundary conditions and a special "dual basis" must be employed to achieve orthogonality of an eigenfunction expansion for the Green's function. For two dimensions, the problem can also be obviated by operational procedures using exponential Fourier transforms. In three dimensions, the orthogonalization process appears to be the most practical approach for obtaining the Green's function.

III. Results

In order to fully appreciate the computational results, a qualitative understanding of the canard-wing flow behavior is in order. Figure 4a schematically shows the effect of canard on the wing by considering the canard as a concentrated vortex Γ_C in front of the wing. This produces a downwash U_d in the wing field thus decreasing the effective angle of attack for the wing ($\bar{\alpha}_W$). As a result the lift on the wing would be lower than that produced by it in isolation. Similarly, the circulation Γ_W produced by the wing as shown in Fig. 4b, induces an upwash U_u in the canard field thus increasing the canard angle of attack ($\bar{\alpha}_C$) which results in larger lift than that which would be produced by it in isolation. The sketches as shown in Figs. 4a and b assume positive lift on both lifting elements.

A canard-wing case was run using an 85×60 grid in each computational region (wing and canard domain). A NACA 0012 profile was used for both airfoils. The canard was placed one wing chord length ($C_W=2$) upstream of the wing airfoil and one wing chord length above. The canard chord was chosen to be 60% of the wing airfoil chord length ($C_C=1.2$). The angle of attack was 1 deg for both the canard and the wing airfoils and the freestream Mach number was 0.75. Calculations were performed on a CDC 7600 computer requiring approximately 1000 iterations to converge to 10^{-4} accuracy. (This means the maximum change in ϕ between two successive iterations was less than 10^{-4}.)

Figure 5 shows the pressure distribution over both the airfoils. A large supercritical region is formed over the upper surface of the canard, terminated by a shock. As expected, the increase in angle of attack due to upwash produces a larger C_L for the canard ($C_{L_{\text{canard}}}=0.344$ based on its own chord length C_C) compared to an isolated airfoil case. The C_L for an isolated NACA 0012 airfoil at Mach number 0.75 and at angle of attack 1 deg is 0.21. The pressure distribution over an isolated NACA 0012 airfoil is also shown in Fig. 5 by the dotted lines.

The pressure distribution on the wing airfoil is barely supercritical due to the reduction in the wing angle of attack and the resulting lift coefficient $C_{L_{\text{wing}}}=0.148$ is also lower than the isolated airfoil case.

Figure 5 also shows a comparison with the results obtained from a linear theory analysis using surface vortex distribution on an aspect ratio 100 rectangular canard-wing arrangement. The square symbols denote the upper surface pressure and the circles denote the lower surface pressure distribution. Linear theory by its nature cannot produce shocks and as a result, cannot give realistic answers when shocks are present on the airfoil. But for sufficiently subcritical flows, it is anticipated that linear theory should compare favorably with the transonic equation results. This can be seen in Fig. 5. Here, the lower surface of both the canard and the wing produce only subcritical Mach numbers and the pressure distribution from the two theories correlate reasonably well. However, on the upper surface of the canard where a strong shock is present, linear theory is grossly inadequate on the forward part of the airfoils.

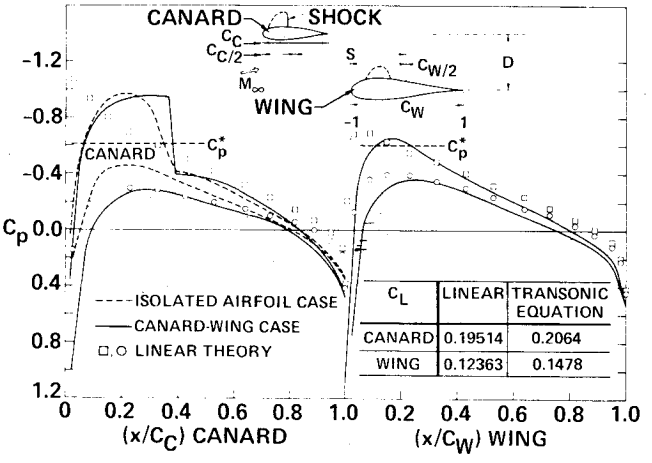

Fig. 5 Pressure distribution over a two-dimensional canard-wing, NACA 0012 airfoils; $M_\infty=0.75$, $\alpha_W=\alpha_C=1$ deg, $S=-2$, $C_C=1.2$, $C_W=2.0$, $D=2.0$.

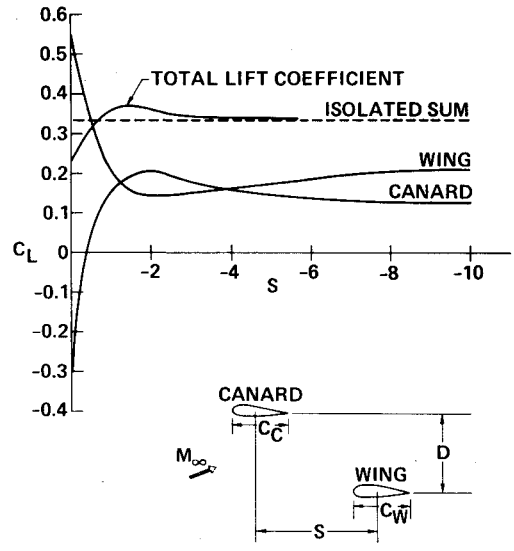

Fig. 6 Variation in lift coefficient with horizontal stagger S; $D=2$, $M_\infty=0.75$, $\alpha_W=\alpha_C=1$ deg, $C_W=2$, $C_C=1.2$.

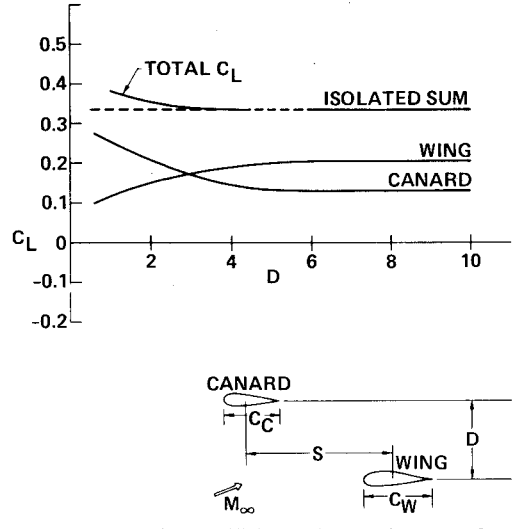

Fig. 7 Variation in lift coefficient with vertical gap D; $S=-2$, $M_\infty=0.75$, $\alpha_W=\alpha_C=1$ deg, $C_W=2$, $C_C=1.2$.

To understand the effect of the relative orientation of both lifting surfaces, a parametric study was conducted in which the location of the canard was varied with respect to the wing. For this study, a total lift coefficient C_L is defined as the sum of C_{LC} and $C_{LW}$where C_{LC} and C_{LW} are the lift coefficients of the canard and the wing (based on wing chord length) under the influence of each other and an isolated lift sum is defined as the sum of $(C_{LC})_I$ and $(C_{LW})_I$ where the subscript I denotes that it is in isolation. When there is beneficial interference the total lift sum C_L will be larger than the isolated lift sum.

The results of the parametric study are plotted and shown in Figs. 6 and 7. Figure 6 shows the variation in lift coefficient with horizontal gap S (stagger) for a fixed vertical gap D. As the canard position moved further away from the wing, the lift coefficients for the wing and the canard rapidly approach their isolated values. When the canard is directly above the wing, $S=0$, the wing produces a large positive lift and the canard produces a large negative lift, as expected. For this case, the induced flow on each airfoil is equivalent to an induced camber of the airfoil. By properly orienting the canard in front of the wing, a net increase of 5-10% in the total lift coefficient can be achieved over the isolated sum because of transonic beneficial interference.

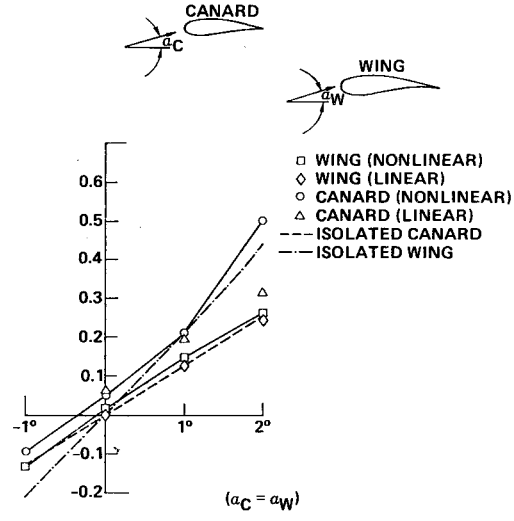

Fig. 8 Lifting effectiveness of canard-wing systems; $S=-2$, $D=2$, $C_C=1.2$, $C_W=2$, $M_\infty=0.75$.

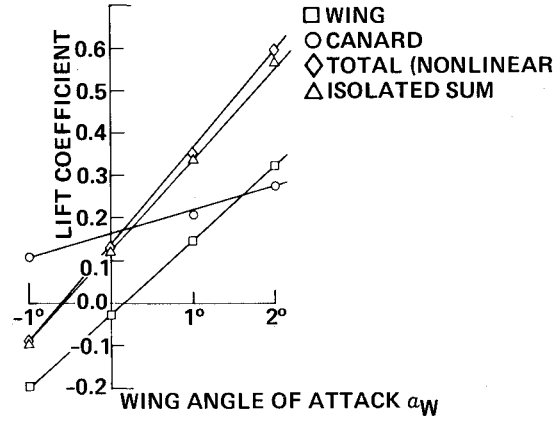

Fig. 9 Effect of differential incidence on canard-wing lift contributions; canard incidence α_C fixed at 1 deg, $C_C=1.2$, $C_W=2$, $S=-2$, $D=2$, $M_\infty=0.75$.

Figure 7 shows a similar lift variation with vertical gap D for a fixed stagger S. Again, as anticipated, when the canard is moved vertically further away from the wing, the lift coefficient approached the isolated case. These studies indicate that for every given Mach number M_∞, angle of attack α_C and α_W there is an optimum location for the canard which would produce a total lift coefficient larger than the isolated sum.

Given any canard-wing staggering arrangement (i.e., S,D,C_C,C_W fixed), it was decided to study how the lift coefficients C_{LW}, C_{LC}, etc., change as the canard and wing angle of attack α_C and α_W are altered by the same amount for a particular Mach number. For a typical canard-wing arrangement ($S=-2, D=2, C_C=1.2$, $C_W=2$, NACA 0012 airfoils) calculations were performed at -1, 0, 1, and 2 deg angles of attack at Mach number 0.75. The results of this study are shown in Fig. 8. When the angle of attack is increased, the canard produces a lift coefficient much larger than the isolated canard case. This is due to the influence of the wing which produces a larger upwash in front of the canard with increasing angle of attack. Similarly, the lift coefficient produced by the wing is much lower than the isolated wing case for increasing angle of attack. Again, this is due to larger downwash produced by the canard in front of the wing. Figure 8 also shows the results from the linear theory. For the larger angles of attack, the linear theory compares very poorly because of its inadequacy to treat shock waves.

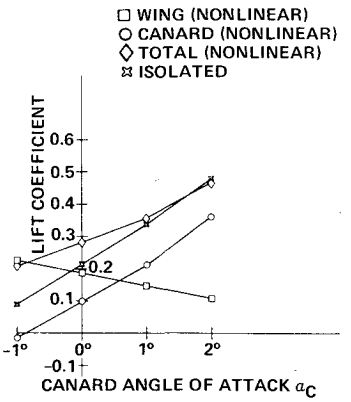

Fig. 10 Effect of differential incidence on canard-wing lift contributions; wing incidence α_W fixed at 1 deg, $C_C = 1.2$, $C_W = 2$, $D = 2$, $S = -2$, $M_\infty = 0.75$.

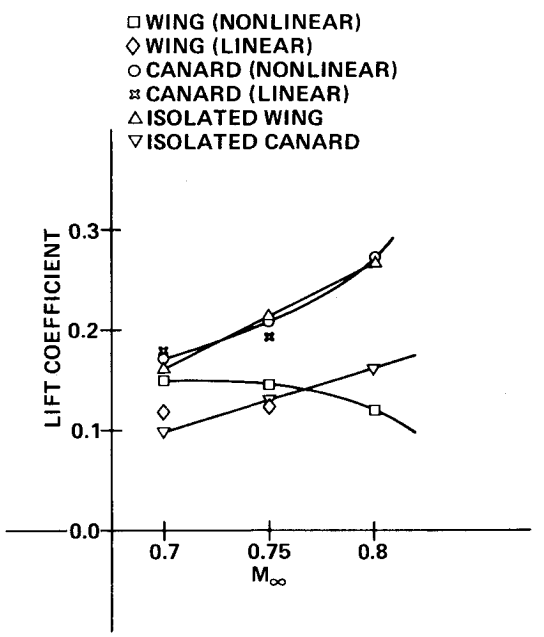

Fig. 11 Mach number effect on canard-wing interference; $\alpha_C = \alpha_W = 1$ deg, $S = -2$, $D = 2$, $C_C = 1.2$, $C_W = 2$.

Figure 9 shows the variation in canard and wing lift coefficients due to changes in the wing angle of attack α_W keeping other parameters fixed ($M_\infty = 0.75$, $\alpha_C = 1$ deg, $C_C = 1.2$, $C_W = 2$, $S = -2$, $D = 2$). As the wing angle of attack increases, the nonlinear total lift coefficient tends to be greater than the isolated sum of the canard and wing lift coefficients. When α_W is negative, the wing produces a negative lift which means a downwash for the canard. Thus, the canard produces a lift coefficient smaller than the isolated value (0.126) when $\alpha_W = -1$ deg.

Figure 10 is a study similar to Fig. 9. Here, the canard angle of attack α_C is varied keeping other parameters fixed ($M_\infty = 0.75$, $\alpha_W = 1$ deg, $S = -2$, $C_C = 1.2$, $C_W = 2$, $D = 2$). The lift on the wing airfoil decreases as the canard angle of attack α_C is increased which results in larger downwash for the wing.

Figure 11 shows the variation in the canard-wing lift coefficients due to change in Mach number keeping other parameters fixed ($\alpha_C = 1$ deg, $\alpha_W = 1$ deg, $S = -2$, $D = 2$, $C_C = 1.2$, $C_W = 2$). It is interesting to note that when the Mach number is increased, the wing produces a smaller C_{LW} (in isolation the airfoil would produce larger C_L as Mach number is increased). As the Mach number is increased the canard produces a much larger lift coefficient than its isolated value.

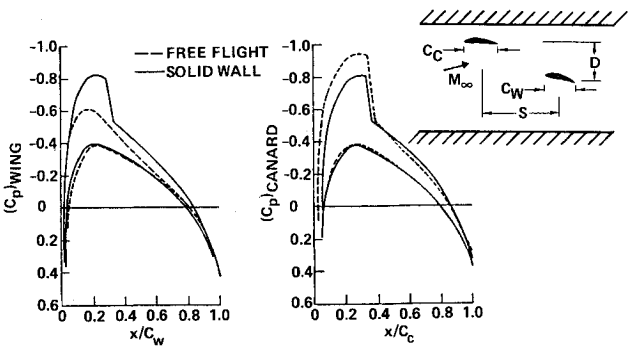

Fig. 12 Comparison of free flight and solid tunnel wall, pressure distributions; $M_\infty = 0.75$, $\alpha_W = \alpha_C = 1$ deg, $H/C_W = 3.75$, $S = -2$, $C_W = 2$, $C_C = 1.2$, $D = 2$.

All of the previous calculations are appropriate to a free flight environment. A typical canard-wing configuration was also analyzed using solid wall boundary conditions and the appropriate far-field conditions given by Eq. (10). The results of this calculation are shown in Fig. 12, which suggest that the choking effect of the solid tunnel walls effectively increases the wing incidence angle, apparently resulting in a larger supercritical region and the addition of a terminating shock. On the other hand, the canard experiences a lower incidence angle compared with the free flight case, and the shock is much weaker. It should be noted however, that this behavior may not be definitive with the possibility of other combinations of the parameters α_C, α_W, H/C_W, M_∞, S, D, C_C, and C_W leading to different trends. Wind tunnel calculations involving slotted and free-jet cases are currently in progress.

IV. Conclusions

The presently developed two-dimensional bi-wing code can be effectively used to study optimum relative locations for both surfaces. For the calculations reported, significant gains in lift have been established by appropriate placement of these surfaces. This should have important implications regarding nonlinear transonic flow effects on stability and control, particularly from the viewpoint of wake downwash effects. Extension of this work on two-dimensional canard-wings to three-dimensional canard-wings is currently in progress, as well as applications to transonic aeroelastic tailoring and flutter of closely coupled multiple-lifting units. In addition, simultaneous design of the interfering system using a new inverse solver[8,12] for both two- and three-dimensional cases represents a future capability.

Acknowledgments

The authors are grateful to W. Clever of the Rockwell Los Angeles Aircraft Division for providing the linear theory results.

A portion of this research was sponsored by the Air Force Office of Scientific Research (AFSC), United States Air Force, under Contract 744620-76-C-0044. The United States Government is authorized to reproduce and distribute reprints for governmental purposes notwithstanding any copyright notations thereon.

References

[1] Re, R.J. and Capone, F.J., "An Investigation of a Close Coupled Canard as a Direct Side Force Generation on a Fighter Model at Mach Numbers from 0.40 to 0.90," NASA TN D-8510, July 1977.

[2] Lacey, D., "Aerodynamic Characteristics of the Close Coupled Canard as Applied to Low-to-Moderate Swept Wings," Vol. 2: *Subsonic Speed Regime,* David Taylor Model Basin Rept. DTNSRDC 79/002, Jan. 1979.

[3] Murman, E.M. and Cole, J.D., "Calculations of Plane Steady Transonic Flows," *AIAA Journal,* Vol. 9, Jan. 1971, pp. 114-121.

[4] Jameson, A., "Iterative Solutions of Transonic Flows over Airfoils and Wings, Including Flows at Mach 1," *Communications of Pure and Applied Mathematics,* Vol. 27, 1974, p. 283.

[5] Murman, E.M., "Computation of Wall Effects in Ventilated Transonic Wind Tunnels," AIAA Paper 72-1007, 1972.

[6] Smithmeyer, M.G. and Murman, E.M., "Far Field Boundary Conditions for Airfoils in Transonic Wind Tunnels," Flow Research Rept. 78, Flow Research Co., Kent, Wash., Dec. 1976.

[7] Pinzola, M. and Lo, C.F., "Boundary Interference at Subsonic Speeds in Wind Tunnels with Ventilated Walls," AEDC TR-69-47, May 1969.

[8] Shankar, V., Malmuth, N.D., and Cole, J.D., "Computational Transonic Airfoil Design in Free Air and a Wind Tunnel," AIAA Paper 78-103, 1978.

[9] Baldwin, B.S., Jr., Turner, J.B., and Knechtel, E.D., "Wall Interference in Wind Tunnels with Slotted and Porous Boundaries at Subsonic Speeds," NASA TN 3176, 1954.

[10] Murman, E.M., Bailey, F.R., and Johnson, M.L., "TSFOIL, A Computer Code for Two-Dimensional Transonic Calculations Including Wind-Tunnel-Wall Effects and Wave-Drag Evaluation," *Aerodynamic Analysis Requiring Advanced Computers,* NASA SP-347, March 1975, pp. 769-788.

[11] Catherall, D., "The Computation of Transonic Flows Past Airfoils in Solid, Porous or Slotted Wind Tunnels," *Wind Tunnel Design and Testing Techniques,* AGARD-CP-174.

[12] Shankar, V., Malmuth, N.D., and Cole, J.D., "Computational Transonic Design Procedure for Three-Dimensional Wings and Wing-Body Combinations," AIAA Paper 79-0344, 1979.